Lunar Power Sources: An Opportunity to Experiment

aerospace

MDPI

Article

Lunar Power Sources: An Opportunity to Experiment

Michele Marrone [1], Luca Pasqualin [2] and Carlo Giovanni Ferro [2,*]

[1] Department of Aerospace Science and Technology, Politecnico di Milano, Via Giuseppe La Masa, 34, 20156 Milano, Italy
[2] Department of Mechanical and Aerospace Engineering, Politecnico di Torino, C.so Duca degli Abruzzi 24, 10129 Torino, Italy
* Correspondence: carlo.ferro@polito.it

Abstract: This paper presents a systematic analysis of power generation technologies for a lunar outpost supporting six astronauts. Based on a detailed power budget analysis requiring 65 kWe for life support, scientific equipment, and in situ resource utilization (ISRU), a comparative analysis of solar and nuclear power solutions is conducted. Nuclear fission is identified as the most promising technology based on key criteria, including mass efficiency, reliability, and power density. A parametric study is then conducted to optimize the nuclear reactor design, with particular focus on radiation shielding using lunar regolith and its impact on safety distances. The analysis demonstrates that proper shielding can reduce the required safety distance from over 2.5 km to approximately 90 m while maintaining radiation exposure within acceptable limits. Finally, leveraging insights from existing reactor designs, an optimized configuration is proposed that combines multiple small reactors to meet the unique challenges of lunar power generation while ensuring crew safety and operational redundancy.

Keywords: lunar outpost; power generation; nuclear fission

Academic Editors: Marco Sabatini and Leonard Felicetti

Received: 24 December 2024
Revised: 9 January 2025
Accepted: 13 January 2025
Published: 16 January 2025

Citation: Marrone, M.; Pasqualin, L.; Ferro, C.G. Lunar Power Sources: An Opportunity to Experiment. *Aerospace* **2025**, *12*, 58. https://doi.org/10.3390/aerospace12010058

1. Introduction

The exploration of lunar environments represents a critical frontier in contemporary space research, with an increasing international focus on establishing a sustainable human presence beyond Earth. In particular, the lunar South Pole has emerged as the premier destination for future missions due to its permanently shadowed craters containing water ice deposits. Through the Artemis program, the United States plans to return humans to the Moon by April 2026, aiming to establish a sustainable presence by 2028. This initiative includes the construction of the Gateway space station in lunar orbit, which will serve as a staging point for missions to the Moon and beyond. The long-term goal is to establish a permanent lunar base [1,2]. Similarly, China has outlined its lunar ambitions with plans for a first crewed landing in 2029, followed by a more comprehensive presence through the International Lunar Research Station (ILRS). This joint venture with Russia aims to establish a robust research outpost near the south pole of the Moon by 2036 [3]. Meanwhile, the European Space Agency (ESA) is enhancing its lunar exploration efforts by participating in NASA's Artemis missions and developing its Argonaut program. Through Argonaut, ESA aims to create a lunar lander capable of transporting cargo to the Moon's surface, representing a significant contribution to the broader Artemis initiative with the first launch planned for 2031 [4,5]. Furthermore, JAXA (Japan Aerospace Exploration Agency) is collaborating with NASA on the Artemis program, focusing on robotic exploration and developing a pressurized lunar vehicle [6]. Japan is set to become the second country, after

the United States, to have a citizen set foot on the Moon. Finally, India has announced plans to send humans to the Moon by 2040, as communicated by Indian institutions [7]. These ambitious lunar exploration plans face unprecedented environmental complexities that challenge conventional power infrastructure. Characterized by extreme temperature variations at the equator ranging from −233 °C during extended lunar nights to 127 °C under direct solar radiation, the Moon demands innovative energy solutions that can operate with unprecedented reliability and adaptability. The topographical peculiarities of potential exploration sites, particularly near the lunar South Pole, further complicate the design of the energy infrastructure, with complex patterns of illumination created by rugged terrain and the low angular trajectory of the Sun [8]. Contemporary lunar power generation strategies focus mainly on two technological approaches: solar panels and nuclear fission reactors [9–11]. Each methodology presents distinct advantages and limitations.

1.1. Solar Panels

Solar power offers potential benefits, including the possibility of utilizing in situ resource utilization (ISRU) for cell production while simultaneously presenting challenges related to extended periods of darkness and location-specific illumination constraints. Despite these operational constraints, photovoltaic technology's extensive heritage in terrestrial and orbital applications establishes it as a highly viable candidate for extraterrestrial power generation. The minimal maintenance requirements and absence of moving components contribute to its operational robustness in extreme environments. Furthermore, advances in thin-film photovoltaics, multi-junction cells with enhanced quantum efficiency, and radiation-hardened designs have significantly improved performance metrics in space applications.

1.2. Nuclear Fission

Nuclear fission, conversely, provides a potentially more consistent power generation approach that could mitigate some of the intermittency issues associated with solar technologies. Furthermore, nuclear fission systems are gaining attention as a promising solution for space propulsion, particularly through the application of nuclear electric propulsion (NEP). NEP systems employ the power generated by nuclear reactors to drive electric thrusters, such as ion or Hall-effect propulsion systems. These propulsion methods offer higher efficiency compared with traditional chemical rockets, especially for missions requiring prolonged thrust and high efficiency, such as interplanetary travel. By providing continuous thrust over extended periods, NEP systems are well suited for missions to distant destinations like Mars and beyond.

Given these advantages, several international initiatives are advancing NEP technology development. In particular, NASA's Kilopower project leads research into compact reactor designs suitable for space applications [11], while the European Space Agency's RocketRoll [12] program focuses on integrating nuclear power with ion thrusters for deep space missions. These programs share common challenges in developing high-temperature materials, efficient power conversion systems, and radiation-tolerant electronics.

1.3. Contents Outline

The selection of an appropriate power generation system extends beyond purely technical considerations to encompass crucial safety factors for human presence. The lunar environment presents significant radiation challenges due to the absence of a protective atmosphere. While nuclear power systems could provide reliable energy, they introduce additional radiation considerations that must be carefully evaluated against background radiation levels and overall mission safety parameters. Nevertheless, the successful development of a lunar power system depends not only on the choice of technology but also on

its spatial configuration and integration with other base systems. This interconnected nature necessitates a comprehensive approach from the initial design phase. To address these complexities, this paper presents a systematic analysis through the following structure:

1. Power requirements analysis: Section 2 establishes a comprehensive power budget for a six-person lunar base, defining the baseline energy demands that must be met.
2. Technology assessment: Section 3 evaluates potential power generation solutions, with Sections 3.1 and 3.2 presenting a comparison between solar and nuclear technologies. This analysis, incorporating preliminary sizing calculations, leads to the selection of nuclear power as the optimal solution. Section 3.3 examines three specific reactor designs from literature that align with the established power requirements.
3. Safety and configuration analysis: Section 3.4 develops a detailed model of the nuclear reactor system, with particular emphasis on safety parameters and the relationship between reactor quantity, positioning, and base layout.
4. Optimization studies: Section 4 presents four parametric studies utilizing the model developed in Section 3, exploring key design variables and their impact on system performance.
5. Optimized design and reality: Section 5 presents the optimized parameters designed to meet the requirements. It also discusses how the existing design can only partially achieve these results.
6. Conclusion: Section 6 presents a summary of the findings of this work as well as some useful recommendations.

Through this systematic approach, the paper aims to develop a comprehensive understanding of the technical and safety considerations necessary for implementing a reliable power generation system for lunar habitation.

2. Power Budget

To estimate the power budget required for a six-person lunar base, data available in the literature [13] are utilized, and additional estimates are derived by combining research findings with logical reasoning to obtain a comprehensive understanding of the energy demands. Firstly, the power budget of a lunar station must account for the contributions from two different types of power sources:

1. Constant power: used to power main electrical circuits that distribute energy across the lunar base, supporting critical systems such as life support, communication, and the proper functioning of scientific equipment.
2. Intermittent power: subjected to peaks, employed for non-permanent activities, like Extravehicular Activity (EVA) operations, rover charging, and ISRU.

In Table 1, each segment is reported with the estimated power required and the safety factor employed. In particular, the safety factors are chosen based on the uncertainty about the associated activity power consumption, according to the following criterion:

- A safety factor equal to 1.2 is applied to activities described in other papers concerning lunar settlement projects, since the availability of numbers and figures extracted is supposed to be highly reliable.
- A safety factor equal to 2 is applied to activities whose power budget is confirmed by experimental tests conducted at Politecnico di Torino to take into account several potential error sources, such as environmental conditions or final binder–regolith composition.
- A safety factor equal to 5 is applied to activities that are foreseen to be carried out in situ, but not enough information is found in space-related literature to derive a quite precise estimation. Typically, power values are defined by referring to different

machinery for similar purposes on Earth or by relying on reasonable guesses. In any case, the contribution of these activities to the overall power budget is not highly impactful; thus, a more conservative approach seems to be appropriate.

Particular attention is given to ISRU activities, as essential to encourage human permanence in the lunar environment.

In the end, to be conservative, a total power budget of 65 kWe is considered, resulting from the simultaneous combination of constant power and total intermittent power (safety factors included).

Table 1. Power budget estimated for a six-human lunar base [14–17].

Power	Activity	Value	Safety Factor
Constant power	Housekeeping [14]	5	×1.2
	Lighting [14]	0.5	×1.2
	Life Support [14]	16	×1.2
	Communication [14]	1	×1.2
	Scientific equipment [14]	2	×1.2
	Total 1	24.5 kWe	29.4 kWe
Intermittent power (peak powers only)	Crew support [14]	17.9	×1.2
	EVA floodlights [14]	2	×1.2
	Rover charging [14]	3	×1.2
	ISRU activity:		
	- Scoop and delivery conveyors [9]	0.2	×5
	- Manufacturing of bricks	0.3	×2
	- Quality control	0.1	×5
	- Assembly of bricks	0.2	×5
	- Health monitoring system [15]	0.5	×5
	- Tool movement system	0.5	×5
	Total 2	24.7 kWe	35.6 kWe
	Total	49.2 kWe	65 kWe

3. Methodology

To determine the technology that best fits the defined power budget, a preliminary sizing of the power system using either solar panels or a nuclear fission reactor is conducted. At the conclusion of this phase, the optimal technology is selected, and a detailed sizing will be carried out for the chosen technology, along with a literature review on it.

3.1. Solar Panels

Solar energy technology, with its widespread terrestrial adoption and continuous efficiency improvements, presents itself as a natural candidate for lunar power generation. However, the Moon's unique environment necessitates a thorough evaluation of this technology's potential and limitations.

The lunar day–night cycle poses a significant challenge, with approximately half of each lunar day spent in darkness. Consequently, solar panels may only be partially effective in meeting the energy demands of a lunar base, necessitating the consideration of substantial energy storage systems. This challenge is inherent and remains unchanged regardless of the base's location on the Moon.

The planned locations for the Artemis missions and future lunar outposts add another layer of complexity. The most promising sites for habitation and scientific exploration, notably the Lunar South Pole and the vicinity of the Shackleton crater, pose unique challenges and opportunities. At a latitude of 89.67° S and a longitude of 129.78° E [18], the Shackleton

crater offers the potential for high concentrations of water ice, making it a suitable location for an outpost. At this extreme latitude, the Sun's low angular elevation of just 1.5° creates complex illumination patterns. However, this unique feature also presents a key advantage: the minimal temperature fluctuations between lunar day and night, which are around 100 °C—significantly lower than the 400 °C experienced at the lunar equator—simplify the selection of materials for infrastructure [9]. Notably, there are permanently shadowed regions where sunlight never reaches the surface, making these areas unsuitable for solar panels [8]. As a result, solar panels must be installed in alternative locations.

Furthermore, even in non-permanently shadowed areas, illumination may be lower than expected due to the irregularities in the terrain. Therefore, a thorough analysis of the lunar topography [8] is crucial for the effective placement of solar arrays. NASA has also investigated alternative approaches to ensure the feasibility of solar panels on the Moon, such as the Transformers for Extreme Environments project [10].

In this context, we conduct a best-case scenario analysis comparing solar and nuclear energy solutions. To establish a clear baseline for comparison, we consider an idealized scenario where terrain irregularities are not taken into account. This approach is particularly valuable because if nuclear reactors demonstrate superior performance even against this optimized solar energy scenario, it provides a definitive basis for technology selection.

Preliminary Sizing

In sizing a solar panel system integrated with battery storage for lunar applications, data and formulas provided by [9] are employed. For transparency and completeness, key formulas are explicitly presented in this analysis. The best-case scenario, as anticipated, treats the Moon as a perfectly smooth sphere, disregarding elevation variations of lunar terrain. This simplification allows for a more straightforward initial assessment. The primary focus of this sizing exercise is on two critical factors: mass and volume. These parameters significantly impact the mission's economic viability, given the considerable cost of transporting all system components from Earth to the Moon. To streamline the design process, the number of free variables is limited. Specifically, the solar panel area is treated as the primary variable, while other parameters such as materials, fill factor, and panel inclination angle relative to the lunar surface are fixed. These predetermined parameters are detailed in Table 2 [9].

The total mass of the system is calculated as the sum of the battery and solar array mass. While a comprehensive design would include additional components such as wiring and electrical management systems, focusing on the battery and solar array—typically the most massive components—provides a sufficient basis for informed decision-making at this stage. Similarly, the computation of whole mass for nuclear reactors considers only the balance of plant, shields, and reactor bulks, by neglecting the contribution given by wiring. Even if the major distances required for safety reasons with respect to the solar array solution could impact the final choice of technology, later results proved a possible consistent reduction in safety distance in case of appropriate shielding techniques, making the effect of wiring upon the overall mass budget not crucial to determine a change in technology. Therefore, wiring mass is not assessed in both cases.

Given these assumptions and simplifications, the following computations aim at computing the mass and volume of the system given the budget information from Table 1. To calculate the power output, it is necessary to compute the hour angle (θ), the lunar declination angle (ψ), and the solar elevation angle (α) for the specific day and hour, which is reported in Figure 1. While the formulas for these angles are omitted for brevity, the equation for the power produced by the array as a function of these angles is included. The sizing is performed for the worst-case scenario, which corresponds to the day of the

year with the shortest illumination period. This approach ensures that the system can meet power requirements even in the most challenging conditions.

Table 2. Summary of parameters [9].

Parameter	Value
Fill Factor (f_{sc})	0.89
Solar Cell Efficiency (η_{sc})	0.28
Latitude (ϕ)	89.67° S
Array Inclination Angle (β)	30°
Maximum lunar declination angle ($\psi_{\max}$)	1.5°
Irradiance [W/m^2] (I_s)	1366
Percentage of Dust coverage (χ_d)	0
Average Space between arrays [m] (S_a)	3
Battery specific energy [kWh/kg] (S_b)	0.2
Battery depth of discharge (B_{dod})	0.8

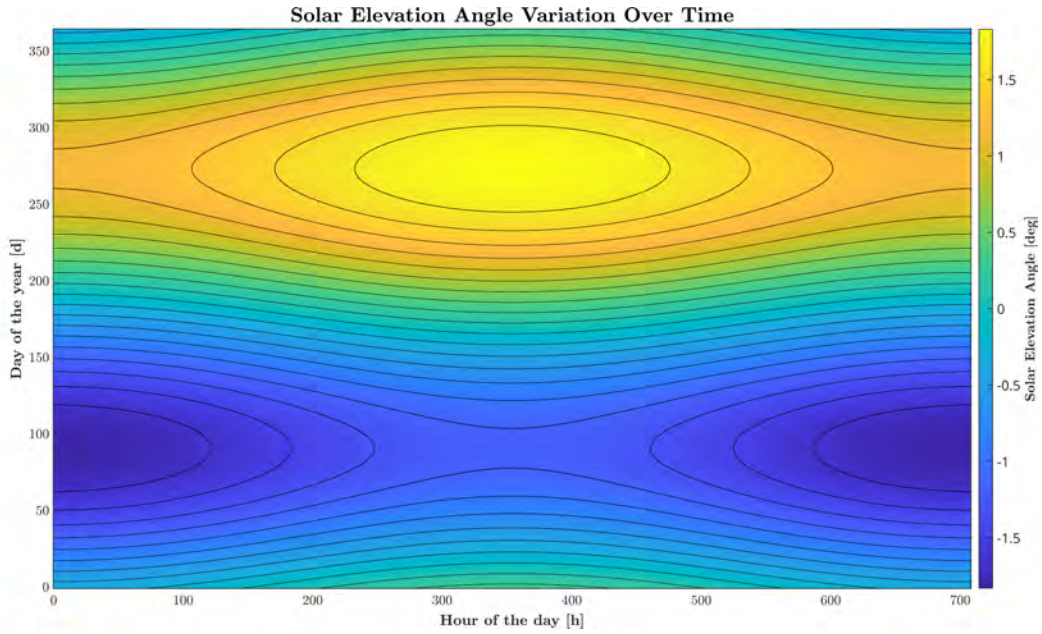

Figure 1. Solar elevation angle versus hour of the day versus day of the year.

The following iterative process is employed to determine the optimal solar array area (A_a):

1. The power generated by the solar array during daytime is given by

$$P_a = (1 - \chi_d) f_{sc} \eta_{sc} A_a I_s \sin(\alpha + \theta) \tag{1}$$

2. The total energy available during the lunar day period is

$$E_a = P_a t_{day} \tag{2}$$

where t_{day} represents the duration of the lunar day.

3. The lunar day is divided into two phases:
   - Daytime phase (t_{dt}) with power requirement P_{dt}.
   - Nighttime phase (t_{nt}) with power requirement P_{nt}.

   Note: The transition to nighttime phase occurs when the solar array output drops below the minimum power requirement specified in the power budget.

4. The energy requirements for each phase are

$$\begin{aligned} E_{dt} &= P_{dt} t_{dt} \\ E_{nt} &= P_{nt} t_{nt} \end{aligned} \tag{3}$$

5. The energy available for storage in the battery system is

$$E_{bat} = (E_a - E_{dt}) \eta_{bat} \tag{4}$$

where $\eta_{bat} = 0.98$ is the battery storage efficiency.

Upon determination of the solar array area, the parameters in Table 2 can be optimized. Then, by choosing the areal density of the arrays(ρ_{arr}), their mass can be computed. Here, ρ_{arr} is taken equal to 1.59 $\frac{\text{kg}}{\text{m}^2}$ [9], hence the mass of the array M_{arr} given by is $A_a \rho_{arr}$.

At this point, the battery mass can be computed as well. Assuming a battery-specific energy S_b and a depth of discharge B_{dod}, the battery mass is computed as follows:

$$M_{bat} = \frac{E_{bat}}{S_b B_{dod}}. \tag{5}$$

Eventually, the total mass can be computed to have a preliminary estimation of the mass of the system.

$$M_{tot} = M_{bat} + M_{arr}. \tag{6}$$

The derived formula enables a mass budget comparison between solar panel systems and nuclear reactors. Based on power requirements outlined by Ross and Ruppert [8], the nighttime power demand is 29.4 kWe, while the daytime demand (combining constant and intermittent power needs) is 65 kWe. Based on the required power, the parameters in Table 2, and previously derived formulas, the total mass of the solar power system is calculated to be around 66,000 kg. This mass estimate facilitates high-level analysis of transportation costs and logistics for Earth-to-Moon material transfer. Considering the Argonaut lander as the transportation vehicle, with its current estimated maximum capacity (M_{arg}) of 2100 kg [4], the number of required launches can be computed as

$$n_{\text{launch}} = \left\lceil \frac{M_{\text{tot}}}{M_{\text{arg}}} \right\rceil = 32. \tag{7}$$

Considering Ariane 64 as the launch vehicle, which has been designated by ESA for the Argonaut lunar lander missions, the launch costs can be analyzed. While Ariane 64's launch cost (c_{launch}) is estimated at 75,000,000 €, potential cost reductions through Gateway supply mission synergies and launch vehicle alternatives could reduce this figure. Using an optimistic scenario with a reduction in costs of around 30% to 50,000,000 € per launch, the total delivery cost to the lunar surface is estimated at 1.6 billion €.

It should be noted that these calculations are based on current estimates and may require revision as technology and mission specifications are refined. Furthermore, the potential implementation of ISRU techniques to produce components of the system locally could lead to significant cost reductions in the future.

3.2. Nuclear Fission Reactors

Nuclear fission reactors offer another viable option for generating energy on the Moon, capable of providing the necessary power for sustaining human settlements. In the last decades, various reactor designs have been proposed specifically to support lunar bases, addressing the challenges posed by the Moon's environment while exploiting its peculiar

characteristics. In this context, the case where reactors are placed directly on the lunar surface without any additional shielding is used to estimate the reactor's properties. As will be evident in the following sections, the effect of additional shielding on the overall system mass is not a significant factor in selecting the best technology for the problem being analyzed here.

Preliminary Sizing

From literature, the thermal power generated by a fission reactor is given by the formula:

$$P_{th} = RR \cdot E_r \cdot V, \tag{8}$$

where RR is the reaction rate measured in $\frac{fissions}{\text{cm}^3\text{s}}$, E_r is the energy obtained per fission event measured in $\frac{MeV}{fissions}$, and V is the volume of the nuclear reactor chamber, in cm^3 [19]. By assuming the atom's choice is fixed, Uranium 235, RR, and E_r can be considered constant, yielding:

$$P_{th} \propto V = \frac{M_r}{\rho_r}. \tag{9}$$

At the denominator, ρ_r is a compact way to express $\rho_{U235} \cdot x_{U235} + \rho_{case} \cdot x_{case}$, where x_i refers to the volumetric fraction of the component i in the total (either U-235 or the material for the case). An additional simplification is made, assuming that ρ_r remains constant regardless of the reactor mass. Since ρ_{U235} and ρ_{case} are material-specific constants, this approximation implies a reactor scaling where the volumetric percentages of U-235 and casing remain unchanged.

Then it can be stated, with a clear approximation, that the supplied P_{th} is directly proportional to M_r. By comparing the power and mass budgets of two different nuclear fission reactor's designs [9], the chart in Figure 2 is obtained for preliminary sizing considerations. This chart also includes the other two contributions to the total mass of the plant, calculated similarly: the mass of the shield, M_{sh}, if present, and the mass of the balance-of-plant, M_{bop}. To establish a clear comparison with solar array equipment, the mass related to the balance of plant is considered and defined as the summation of complementary items to the reactors themselves: a primary heat transfer system, including radiators, an intermediate heat and storage system, and a power conversion system [20]. For a given P_{th}, the total mass of the plant (considering one reactor without a shield) can be determined as follows:

$$M_{tot} = M_r + M_{sh} + M_{bop} = M_r + M_{bop}. \tag{10}$$

Attention must be paid to the type of power being considered (P_{th}), which is significantly higher than the net electrical power (P_{el}) actually achieved. Typically, $P_{el} = \eta P_{th}$, where the conversion efficiency, $\eta \approx 0.25$ [9]. Preliminary calculations based on observed trends indicate that for $P_{th} = 4 \times 65 = 260$ kWth, the total mass would be $M_{tot} = 7900$ kg if accounting for the effect of shielding, or even less if not, resulting in $M_{tot} = 5200$ kg. Although these values may be subject to errors due to linearization, it clearly demonstrates that choosing a nuclear plant as the primary energy source is preferable to solar panels. The overall mass is an order of magnitude lower, with the total mass of the solar array system estimated at around 66,000 kg. Consequently, a model for the nuclear plant designed for a six-person settlement will be presented in the following sections, while the use of solar arrays is excluded.

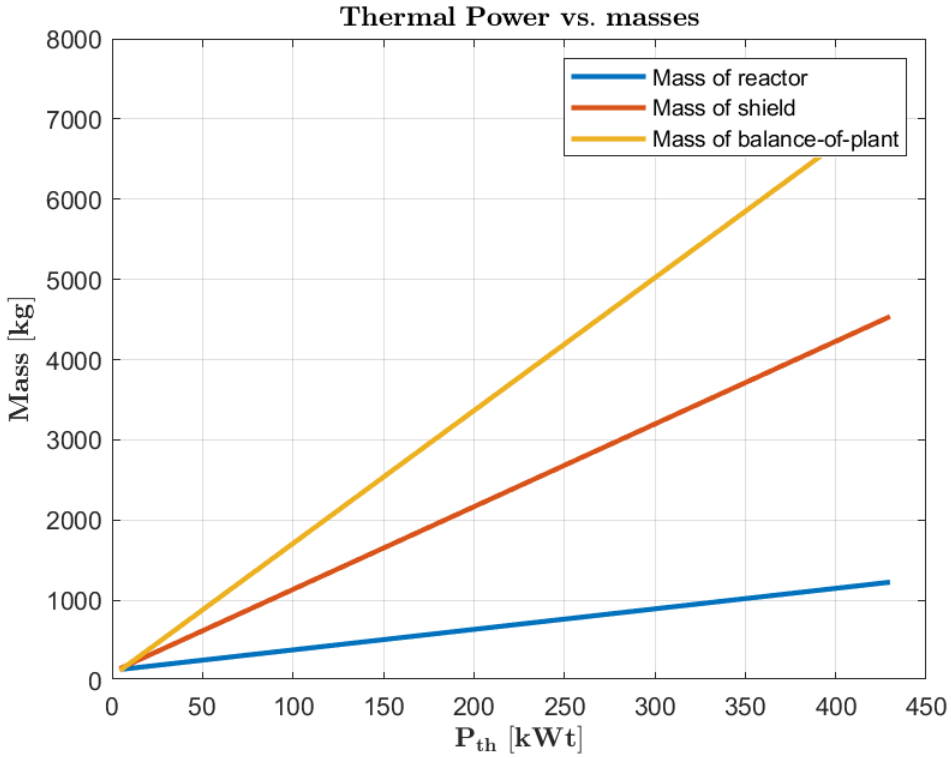

Figure 2. Graph of linear interpolation between the three main different contributions to the reactor mass, M_r, M_{sh}, and M_{bop}, as a function of thermal power generated.

3.3. Overview of Nuclear Reactors

In this context, a review of several of these solutions is presented, followed by an evaluation of their key characteristics. However, it has to be recognized that the review may not comprehensively address all aspects of each solution due to the limited technical details available in the literature.

Additionally, it is important to note that while this assessment concentrates on space-specific designs, the field of nuclear power for extraterrestrial applications is rapidly evolving. Although many current terrestrial reactor designs could potentially be adapted for lunar or Martian outposts, they have not been included in this study.

The evaluation will take into account several critical factors. These include power output capacity, mass and volume constraints, radiation shielding, and operational lifespan. The aim is to assess existing solutions in order to identify the most promising designs that could fulfill the needs of a lunar outpost.

The solutions discussed in this review are selected based on their innovation and level of detail. Projects resulting from collaborations between NASA and the DOE (U.S. Department of Energy) typically provide more comprehensive information. Conversely, projects from other agencies may have limited available data or be too recent for extensive information to be accessible.

This review does not include every NASA project proposed in the past two decades, as many earlier initiatives are surpassed by more advanced studies. However, for completeness, a comprehensive list of all the projects known to the authors is presented. This list also underscores the foundational efforts that have influenced the projects to be discussed.

In particular, a chronological list of projects not extensively detailed in this review is presented in Table 3, with dates based on the publication dates of the cited papers in the bibliography.

Table 3. Reactor specifications ordered by year. P = power, M = mass, SM = specific mass.

Reactor	P (kWe)	M (kg)	SM (kg/kWe)	Year	Maturity Level
SP-100 [21]	100	-	40–45	1980s	Component Testing
HOMER-25 [22]	25	1564	62.6	2000	Component Testing
SAFE-400 [23]	100	541	5.4	2002	Conceptual
SPARS [24]	100	2374	23.7	2003	Conceptual
MSR [25]	100	4525	45.3	2004	Conceptual
SAIRS [26]	4–7	-	-	2004	Conceptual
HP-STMCs [27]	110	-	-	2004	Conceptual
S4 [28]	100	-	-	2005	Conceptual
SUSEE [29]	200	3000	15	2006	Conceptual

The reactors that will be detailed and analysed thoroughly for the MOSS Projects are LEGO [30], SC-SCORE [31], and FSP [32].

3.3.1. LEGO

The LEGO (Lunar Evolutionary Growth-Optimized) reactor is a modular, fast-fission, heat-pipe-cooled clustered reactor system designed for lunar-surface power generation. This reactor system is composed of subcritical units that can be safely launched from Earth and directly emplaced into holes drilled into the lunar regolith, as in Figure 3b, which serves both as radiation shielding and neutron-reflector material. Each subunit, manufactured using proven materials like uranium–dioxide fuel and stainless-steel cladding, utilizes liquid–sodium heat pipes for efficient heat transfer.

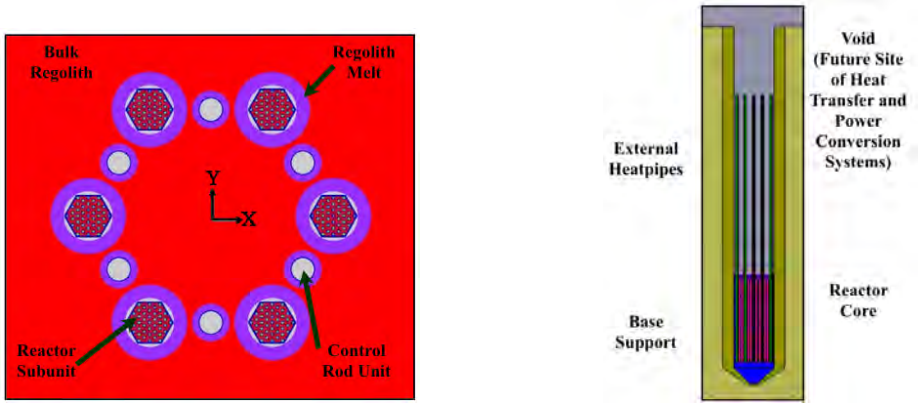

(**a**) (**b**)

Figure 3. LEGO reactor: (**a**) LEGO reactor cluster on the lunar surface; (**b**) Reactor subunit emplaced within the lunar regolith.

The reactor employs a free-piston Stirling engine for power conversion, ensuring a minimum operational lifetime of five years. A single unshielded subunit has an estimated mass of 448 kg and provides approximately 5 kWe, with a height of 8.77 m and a diameter of 0.50 m when fully extended.

The system is designed to promote safety, reliability, and ease of manufacture, with a single cluster of six subunits, depicted in Figure 3a, capable of generating around 30 kWe. As lunar base development progresses, additional subunits can be added to meet increasing power demands.

The LEGO reactor's modular approach aligns with NASA's incremental build strategy, enhancing mission safety by reducing the impact of any single launch failure on the overall power system.

3.3.2. SC-SCORE

The Solid Core-Sectored Compact Reactor (SC-SCORE) is designed to provide continuous power generation for lunar outposts, offering a nominal 38 kWe for approximately 21 years. This monolithic-core reactor operates at a thermal power of 1.0 MWth and consists of six sectors. Each sector is neutronically and thermally coupled but hydraulically independent, featuring separate primary and secondary cooling loops, thermoelectric (TE) powered electromagnetic pumps, TE power conversion assemblies, and heat pipe radiator panels. The reactor core, made from 316L stainless steel or oxide dispersion strengthened molybdenum (ODS-Mo), uses highly enriched uranium nitride (UN) fuel, which provides high thermal conductivity and reduces operating temperatures. The SC-SCORE is emplaced in a 2.5-meter-deep trench below the lunar surface and covered with regolith, which serves as radiation shielding and a supplemental neutron reflector. This configuration protects sensitive equipment and crew from radiation while increasing the reactor's operational lifespan by enhancing core excess reactivity. The reactor's design, whose schematic is reported in Figure 4, ensures safety, with the ability to continue operating at reduced power in the event of a loss of coolant (LOC) or loss of cooling (LOCo) in one sector. Additionally, the SC-SCORE's use of liquid NaK-56 coolant, known for its higher density, heat capacity, and thermal conductivity, ensures efficient reactor cooling and minimizes pressure losses. The SC-SCORE system employs static components with no single point of failure in reactor cooling and energy conversion, promoting reliability and long-term operation.

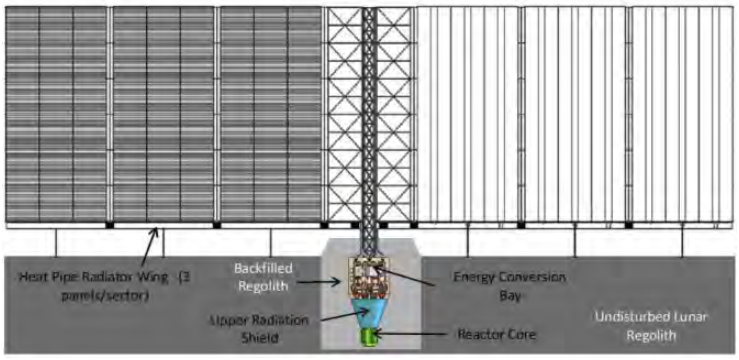

Figure 4. Below-grade SC-SCORE power system with heat pipe radiator panels erected on the lunar surface.

3.3.3. Kilopower and Fission Surface Power Project

The Kilopower project [11], led by NASA, aimed to develop a compact nuclear power system suitable for long-duration space missions. It features a solid uranium-235 core and advanced heat pipe technology capable of generating between 1 to 10 kilowatts of electrical power. This system supports various spacecraft systems, scientific instruments, and potential life support needs during missions to distant celestial bodies. Kilopower's safety and reliability under space-like conditions were validated through rigorous testing, including the successful KRUSTY (Kilopower Reactor Using Stirling Technology) experiment in 2018. This project represents a significant step forward in enabling sustained human exploration and scientific research beyond Earth's orbit.

To meet the increasing power demands for lunar exploration, NASA has expanded this technology under the Fission Surface Power Project. This initiative aims to develop a

deployable 40-kilowatt electric (kWe) Lunar Fission Surface Power Concept, building upon the foundational work of Kilopower [32].

Deployable Reactor

The 40 kWe lunar fission surface power reactor concept in Figure 5 employs several key technical solutions to address the challenges of providing continuous power on the Moon. At its core, the reactor utilizes a high-assay low-enriched uranium (HALEU) fuel design, consisting of 20% enriched uranium nitride (UN) pellets, sodium (Na) - molybdenum (Mo) heat pipes, and a yttrium hydride (YH) moderator. This HALEU approach allows for lower enrichment compared with previous highly enriched uranium concepts while still achieving the required functionality. The reactor is designed to provide approximately 250 kWth to supply the required 40 kWe for a 10-year operational lifespan. Power conversion is achieved through eight 6.2 kWe Stirling converters operating in dual opposed pairs, with a hot end temperature of 700 °C limited by super-alloy material constraints. The thermal control system features a deployable accordion-style radiator based on International Space Station designs, coupled with a pump loop cooling system to transfer heat from the Stirling engines to the radiator. For efficient power transmission over the required 1 km distance, the system employs ±2800 VDC to minimize conductor mass, resulting in a cable mass of approximately 45 kg. The design also incorporates redundancy and fault tolerance, with duplicate components for critical systems such as power distribution units and DC–DC converters. To facilitate deployment, the system is divided into three separate elements: the reactor system, the control system, and the cable and spool system. These elements are designed to be transported and deployed using a pre-existing lunar rover chassis.

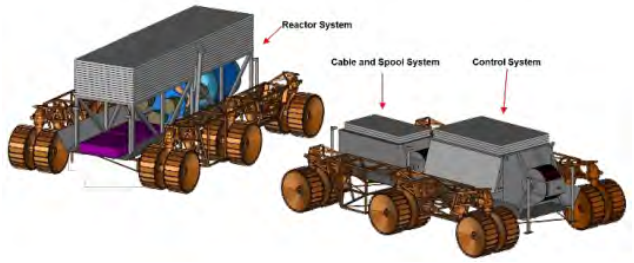

Figure 5. Reactor system, control system, and cable and spool system elements mated to the rover chassis.

3.4. Nuclear Reactors Detailed Modelization

The investigation now considers a variable number of reactors each supplying an equal and fixed thermal power. To assess the relation between the necessary safety distance r_s from reactors and the number of reactors N_r involved, an initial hypothesis is made, confirmed by numerical data shown in [9]. This hypothesis states that the total radiation dose D at a point P from a certain distance r is the sum of the radiation contributions from each reactor at that point. This is the same principle at the basis of the luminous intensity generated by N_l lamps in a room, considered as incoherent light sources [33].

$$D(P) = \sum_{i=1}^{N_r} D_i(P). \tag{11}$$

The intensity of radiation, or radiation dose, follows a quadratic law in a vacuum, as expressed hereafter (D_s is the limit radiation dose for human safety, equal to 5 rem/year, according to the standards for protection against radiation issued by the US Nuclear Regulatory Commission [34]):

$$D = D_s \cdot \left(\frac{r_s}{r}\right)^2. \tag{12}$$

By starting with the human safety constraints detailed in the following sections, an insightful formula can be derived for preliminary considerations, assuming no shielding is present. This formula is applicable under the assumption of N_r nuclear reactors, each generating a constant and uniform amount of power, all positioned at the same distance from point P.

$$D(r_1) = N_r \cdot D_1 = N_r \cdot D_s \cdot \left(\frac{r_s}{r_1}\right)^2 \leq D_s. \tag{13}$$

By simplifying D_s and rearranging the terms in a convenient manner, the following expression is obtained:

$$r_1 \geq \sqrt{N_r} \cdot r_s. \tag{14}$$

Since $r_1 = r_i$ with $i = 1, ..., N_r$, the formula obtained is valid for all the reactors. Moreover, it is known that a 10 kWe reactor generates a radiation dose D^* of 26.3 rem/year at a distance r^* of 500 m [9]; thus, that can be used to compute the actual values of safety distances as a function of N_r. By employing the quadratic law ($N_r = 1$):

$$r_s = r^* \cdot \sqrt{\frac{26.3}{5}} = 1.15 \text{ km}. \tag{15}$$

The meaning of this result is that 1.15 km is necessary between the habitat and the nuclear reactor plants to ensure human safety. This safety distance increases with the square root of the number of reactors, as illustrated in Figure 6.

It is evident that these distance values present significant logistical challenges. Consequently, the focus shifts to exploring potential methods for reducing this distance and quantifying the effect of introducing shielding.

To sum up, the two studies just presented were highly useful to pave the way for the successive steps to take: the former showed to what extent a nuclear fission power plant can be more advantageous with respect to a solar array-based one, whilst the latter demonstrated the importance of introducing a shield for practical and safety reasons. The parametric model developed for this analysis integrates both the nuclear reactor characteristics and the radiation attenuation effects of the regolith shield. This comprehensive approach incorporates multiple degrees of freedom to capture the complex interactions between reactor design and shielding requirements. The detailed methodology and underlying principles of this model, along with its implementation and validation, are presented in the following sections.

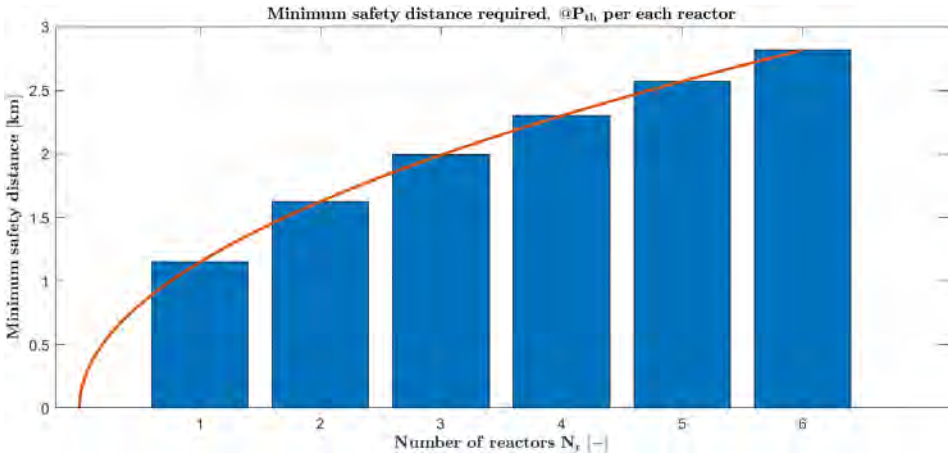

Figure 6. Safety distance required as the number of reactors increases (electric power of a single reactor fixed at 10 kWe). No shield is considered. The red line shows the analytic function $f(N_r) = 1.15\sqrt{N_r}$.

Definitive Methodology: Modelization of the Shielded Nuclear Plant

To analyze the radiation attenuation effects of shielding materials in the nuclear power plant, the following assumptions are adopted:

1. The reactors use Uranium-235 fission to provide power;
2. All the reactors, whose number N_r is a degree of freedom, generate the same amount of power;
3. The reactors are aligned along a line, and the spacing γ between each other is the same for all;
4. The reactors are cylindrical, though this is not a constraint of primary importance;
5. The reactors are installed in a dip; thus, the shielding effect is ensured by the ground regolith itself surrounding the dip. The dip is not covered on the top by a layer of regolith, therefore it is open-vacuum.
6. To adopt a conservative approach, the total radiation from a single reactor is assumed concentrated in the upper central portion of the chamber. This assumption minimizes the impact of attenuation by the regolith, as the radiation travels through the least amount of matter.

The simplified model of the plant is reported in Figures 7–9. All the following reasoning will be based on the nomenclature used in the images.

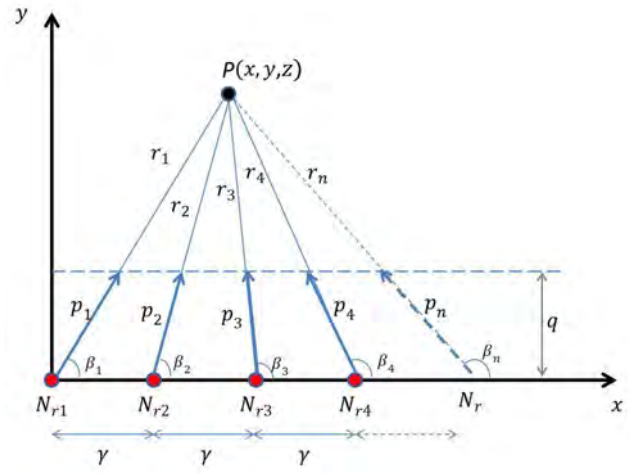

Figure 7. Modelization of the nuclear plant viewed from above (plane xOy).

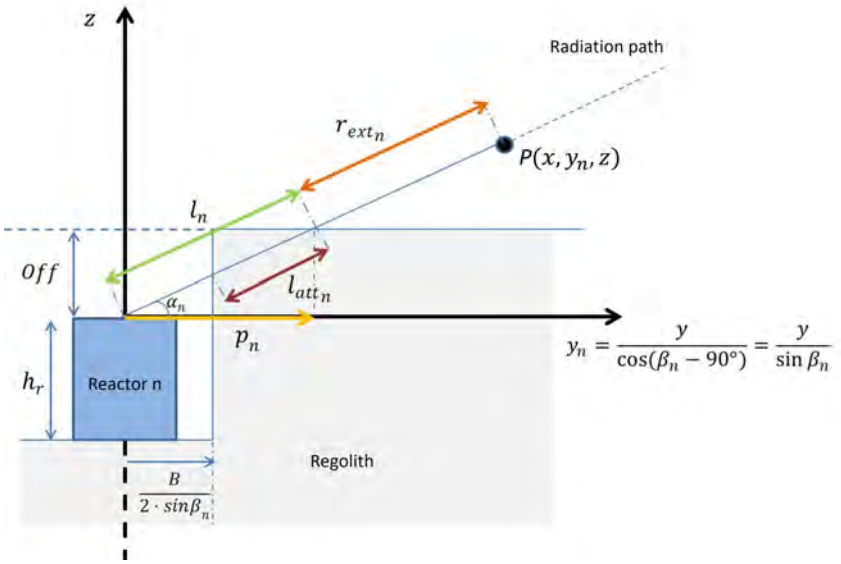

Figure 8. Modelization of the nuclear plant viewed from the side (plane y_nO_nz). Pay attention to the fact that it is the reference system located in the reactor n, so $y_n \neq y$-axis.

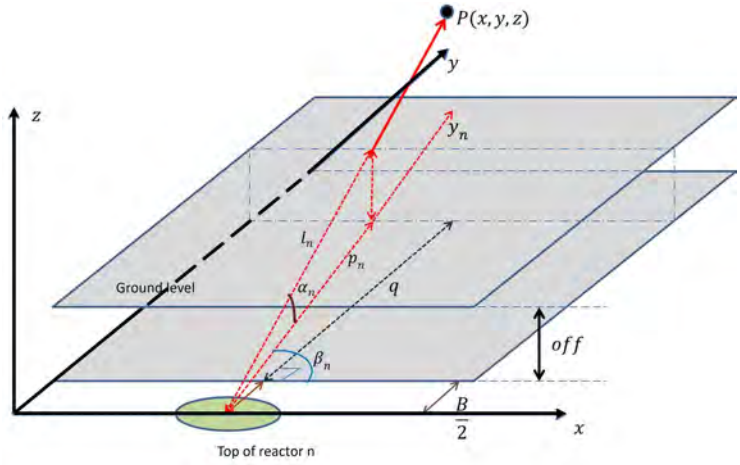

Figure 9. View in perspective of the modelization of the nuclear plant in the 3D space xyz.

The first important point to highlight is the list of degrees of freedom that define the model presented. Each degree of freedom represents an input parameter:

1. $P(x, y, z) \rightarrow$ the generic point where to compute the total radiation;
2. $\gamma \rightarrow$ the inter-distance between two consecutive reactors along the x-axis;
3. $N_r \rightarrow$ the number of nuclear fission reactors in the plant;
4. $off \rightarrow$ the offset between the upper surface of the single reactor and the local lunar ground level;
5. $B \rightarrow$ the width of the dip along the y-axis.

The implementation of the model on MATLAB r2024a aims at achieving, given the inputs previously enumerated, valuable information, listed hereafter:

1. $l_n - l_{att_n} \rightarrow$ the path length of the radiation emitted by the reactor i, with $i = 1, \ldots, N_r$, from the reactor to the first impact with regolith (vacuum);
2. $l_{att_n} \rightarrow$ the path length of the radiation emitted by the reactor i, with $i = 1, \ldots, N_r$, from the first impact with regolith to the end of the regolith, consisting of an attenuation of dose (matter);
3. $r_{ext_n} \rightarrow$ the path length of the radiation emitted by the reactor i, with $i = 1, \ldots, N_r$, from the point where the radiation leaves the regolith to $P(x, y, z)$ (vacuum).
4. D_1, D_2, and $D_3 \rightarrow$ the radiation dose rates are calculated at each segment endpoint, with D_3 at point P being the critical value for determining safety requirements.

To clarify the process, two flow charts representing inputs, outputs, and their connection are reported in Figures 10 and 11. The final objective is to produce a radiation dose map to delineate safe and unsafe regions based on a given set of initial conditions.

By referring to Figure 10 and the top and side views of the plant model shown in Figures 7 and 8, the required quantities can be determined through trigonometric calculations, as outlined below.

1. $\beta_n \rightarrow$ Given $P(x, y, z)$, N_r and γ as inputs, it is quite immediate to get the angle β for each reactor:

$$\beta_n = \begin{cases} \arctan\left(\dfrac{y}{x - (n-1)\cdot\gamma}\right) & if\ x > (n-1)\cdot\gamma \\ \arctan\left(\dfrac{y}{x - (n-1)\cdot\gamma}\right) + \pi & if\ x < (n-1)\cdot\gamma \end{cases} \tag{16}$$

2. $\tan(\alpha_n) \rightarrow$ Given $P(x, y, z)$ and found β_n, by looking at the side view of the model, the values of $\tan(\alpha_n)$ for each n can be computed:

$$\tan(\alpha_n) = \frac{z}{\frac{y}{\sin(\beta_n)}} = \frac{z \cdot \sin(\beta_n)}{y} \implies \alpha_n = \arctan(\tan(\alpha_n)) \tag{17}$$

3. At this point, l_n can be obtained (sum of radiation path 1 and 2, respectively, from the reactor to the regolith wall and from the regolith wall to the ground level):

$$l_n = \frac{off}{\sin(\alpha_n)} \tag{18}$$

4. Since B is established, the effective radiation path length of segment 2, inside the regolith, where the radiation is attenuated, is given by

$$l_{att_n} = l_n - \frac{B}{2 \cdot \sin(\beta_n) \cdot \cos(\alpha_n)} \tag{19}$$

5. The next step is to obtain the values of p_n, an intermediate passage to obtain the expression of r_{ext_n}, which corresponds to the set of radiation path lengths from ground level to the point P, namely the last segment. In formulas,

$$\begin{aligned} p_n &= l_n \cdot \cos(\alpha_n) \\ r_{ext_n} &= \sqrt{\left(\frac{y}{\sin(\beta_n)} - p_n\right)^2 + (z - off)^2} \end{aligned} \tag{20}$$

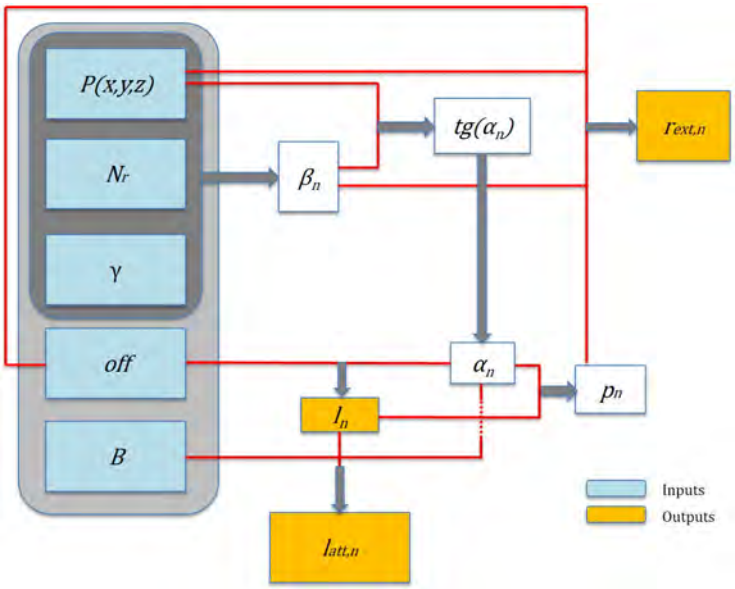

Figure 10. Flow chart of the nuclear reactors' model: from inputs to outputs.

At this stage of the algorithm, the first three outputs (l_n, l_{att_n}, and r_{ext_n}) are available. With these, it is possible to calculate the distances of the entire radiation path from a single reactor, which is divided into three segments: vacuum below the surface, regolith, and vacuum above the surface. Each segment, referred to as S_1 (vacuum below the surface), S_2 (regolith), and S_3 (vacuum above the surface), must be considered separately. Figure 11 illustrates the propagation models used for each segment.

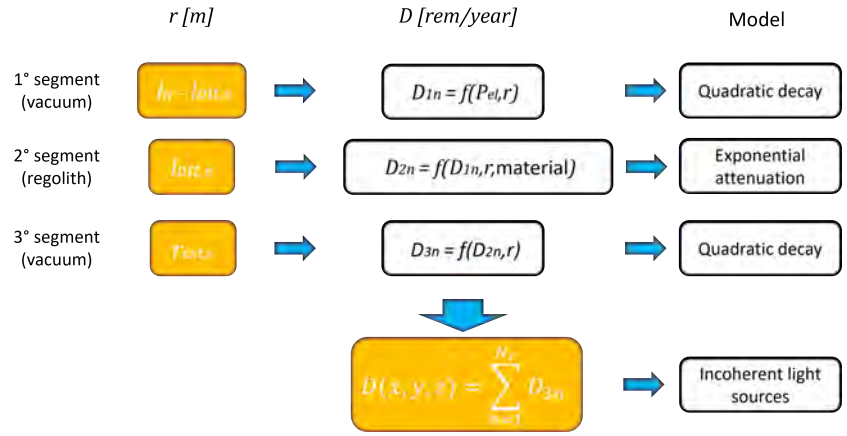

Figure 11. Flow chart describing how to pass from the measurements of lengths to the computation of total radiation dose in point $P(x, y, z)$.

1. $S_1 \rightarrow$ To obtain D_{1n}, the radiation dose due to the n reactor (with $n = 1, ..., N_r$) at the end of S_1, a quadratic decay law could be used since it is in a vacuum. In this case, a chart correlating dose rate and distance by using the power generated as a parameter is necessary: by knowing N_r and the power output of each reactor (since the total power budget is fixed), and using $r = l_n - l_{att_n}$ to locate the value on the graph, D_{1n} can be found.
2. $S_2 \rightarrow$To obtain D_{2n}, since S_2 is formed by regolith, the quadratic law is not applicable. Since the most penetrating particles generated by fission are neutrons and γ rays (the last ones in particular), an exponential attenuation model is employed. The generic expression is given hereafter, where D and D_0 are, respectively, the final and initial doses, while k and x are, respectively, a coefficient depending on the material and the length of the path, that is, l_{att_n} in our case:

$$D = D_0 \cdot e^{-kx}. \tag{21}$$

   By computing k correctly and being D_{1n} already known, D_{2n} can be found as well.
3. $S_3 \rightarrow$ To obtain D_{3n}, that is the radiation dose emitted by the n reactor (with $n = 1, \ldots, N_r$) computed at the end of S_3, the quadratic decay law is applicable since the path is in a vacuum. The lengths are obviously known (both l_n and r_{ext_n} are useful), and D_{2n} as well; hence computing D_{3n} is immediate.
4. Once all the dose contributions given by N_r reactors at point $P(x, y, z)$ are known, the total dose $D_3(x, y, z)$ can be determined by applying the principle of linear addition of doses (similar to the incoherent light sources model).

It is crucial to highlight a key assumption in the analysis: scattering and the production of additional radiation within the regolith are considered negligible. This implies that the regolith is assumed to be an absorbent material that does not influence the direction of the radiation. These assumptions shall be verified through experiments, although additional considerations reveal to be useful to demonstrate a good level of model reliability:

- Based on the studies about regolith shielding properties conducted within the Resolve Program at NASA-Johnson Space Center in 2008 [35], it is clear how the regolith is an excellent material to protect against radiations; thus, it can certainly attenuate them.
- A potential scattering effect is not really a big deal, due to the fact that a deviation could either increase the radiation path inside regolith (reducing even more the radiation dose) or decrease it (in this case, higher radiation path angles with respect to the horizontal plane are obtained, with no direct impact consequences on the habitat).

In general, the introduction of assumptions within the model, always elaborated according to a conservative perspective, can be mitigated by introducing safety margins at the end of calculations.

The human settlement is assumed to be placed at a certain distance along the positive y-axis, whilst what happens for negative values of y is not treated.

S_1: Dose versus distance for different powers.

As previously anticipated, S_1 is covered in vacuum, thus the quadratic decay law can be applied (D_{0n} and r_{0n} are, respectively, dose rate and distance from reactor n, where both the values must be known):

$$D_{1n} = D_{0n} \cdot \left(\frac{r_{0n}}{r_{1n}} \right)^2. \tag{22}$$

In order to derive a relation $P_{el} = f(r)$, which, given a fixed radiation dose, calculates how the electric power delivered affects the distance at which that radiation is measured, a solar radiation analogy is applied [36]. The thermal power P_{th} generated is responsible for the radiation itself and can be written as follows:

$$P_{th} = \int_0^{m_U} \int_0^A \mathcal{P}^* \, dA dm_u = \mathcal{P}^* A m_u. \tag{23}$$

where $\mathcal{P}^*$ is defined as thermal power generated per unit reactor area dA per unit mass of Uranium dm_U computed on the surface of the reactor. This magnitude represents the dose of radiation per unit area emitted through the space, still computed on the surface of the reactor. In fact, if we call $\mathcal{P}^*$ as $\mathcal{D}^*$, this is what is obtained:

$$\mathcal{P}^* = \mathcal{D}^* = \frac{D^*}{A} \quad \left[\frac{W}{\text{kg} \cdot \text{m}^2} \right]. \tag{24}$$

Therefore, by combining (23) and (24):

$$\mathcal{D}^* = \frac{P_{th}}{A m_U} = \frac{P_{th}}{k_s r_{req}^2 m_U}. \tag{25}$$

where k_s is a non-dimensional shape factor, whilst r_{req} is an equivalent reactor radius, depending on the shape of the chamber (for a sphere, the actual radius and the equivalent coincide). By following the procedure explained in [36], it is possible to get, for a generic distance r:

$$\mathcal{D} = \mathcal{D}^* \cdot \frac{k_s r_{req}^2}{r^2} \implies P_{th} = \mathcal{D} m_U r^2 = \frac{D}{A} m_U r^2. \tag{26}$$

If the dose of radiation is fixed as previously imposed and the ratio m_U / A is reasonably assumed to be approximately constant, it is clear that

$$P_{th} \propto r^2 \implies P_{el} = \eta P_{th} \propto r^2. \tag{27}$$

It is determined from [9] that a radiation dose of 26.3 rem/year is measured at distances of 100 m and 500 m from a 1 kWe and a 10 kWe reactor, respectively. Moreover, if the delivered power is null, then also the dose radiation and the distance r converge to zero. These three conditions were useful in order to derive the following empirical quadratic law:

$$P_{el}(r) = 2.5 \cdot 10^{-3} \cdot r(0.01r + 3). \tag{28}$$

By inverting it and considering only the physical solution, with positive values of r, it is finally obtained:

$$r = 10^2(-1.5 + 2\sqrt{0.5625 + P_{el}}). \tag{29}$$

where P_{el} is expressed in kWe and r in m. This last formulation is essential, once P_{el} of the single reactor is fixed, because it yields the distance where the radiation dose is equal to 26.3 rem/year. Therefore, by setting D_{0n} equal to 26.3 rem/year and r_{0n} equal to (29), the product $D_{0n} \cdot (r_{0n})^2$ is a constant for a single reactor. Since this constant can only change through the parameter P_{el} and the hypothesis of N_r equivalent reactors still holds, once P_{el} is fixed, the already written product is a constant for all the reactors involved. The parametric study for different values of electric powers is reported in the chart in Figure 12. In the formula,

$$D_{1n} = 26.3 \cdot \left[\frac{10^2(-1.5 + 2\sqrt{0.5625 + P_{el}})}{r_{1n}} \right]^2, \tag{30}$$

where r_{1n} is set equal to the length of S_1, that is $l_n - l_{att_n}$.

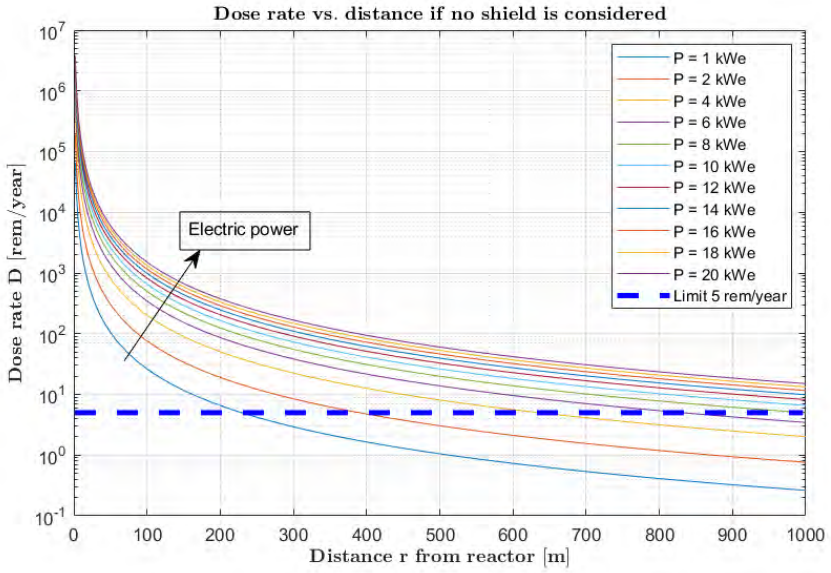

Figure 12. Dose rate as a function of distance from a reactor, with different values of electric power generated by the reactor. The higher the power obtained, the higher the dose is at a fixed distance.

S_2: Exponential attenuation

At this point, the effect provided by the regolith in the attenuation of radiation has to be computed. As previously introduced, an exponential model can be applied:

$$D_{2n} = D_{1n} \cdot e^{-kx} \qquad \text{with } k = \frac{\mu}{\rho} \cdot \rho. \tag{31}$$

Since D_{1n} is known as well as x, which is set equal to l_{att_n}, the only coefficient to be determined is k. This problem requires two quantities to be solved: the estimation of the mass attenuation coefficient $\left(\frac{\mu}{\rho}\right)_{reg}$ for the regolith and the regolith's density ρ_{reg}.

1. $\left(\frac{\mu}{\rho}\right)_{reg} \Longrightarrow$ This is a function of material, number of elements, and energy carried by the radiation. In fact, for a generic compound like regolith, the mass attenuation coefficient can be computed by additivity [37]:

$$\left(\frac{\mu}{\rho}\right)_{reg} = \sum_{i=1}^{N_{el}} \left(\frac{\mu}{\rho}\right)_i \cdot w_i. \tag{32}$$

where w_i is the fraction in weight of element i in the compound. By elaborating on data provided by [38], an average chemical composition of regolith is derived and

reported in Table 4. For all the elements forming regolith, the related coefficient of mass attenuation could be found tabulated as a function of radiation energy. Since neutrons and γ rays represent the most penetrating byproducts and follow a similar exponential law, to be conservative it is assumed that all the energy carried out by neutrons and γ rays is actually employed by only γ rays. It is estimated, with a certain margin of error, a value of 15 MeV per fission inherited by γ rays.

At this point, $\left(\frac{\mu}{\rho}\right)_{reg}$ can be easily computed, resulting in 0.0219 $\frac{\text{cm}^2}{\text{g}}$.

Table 4. Average composition of lunar regolith.

Periodic Element	Weight Fraction
el	$\mathbf{w_i}$ **(%)**
Oxygen (O)	42
Silicium (Si)	21
Iron (Fe)	13
Calcium (Ca)	8
Aluminum (Al)	7
Magnesium (Mg)	6
Others	3

2. $\rho_{reg} \implies$ Since a lower absolute value of the exponent coefficient k corresponds to reduced attenuation, a density close to the minimum, specifically 1.6 $\frac{\text{g}}{\text{cm}^3}$, is selected. This choice assumes a less intense shielding effect and provides a more conservative estimate.

The results are presented as parametric curves in Figure 13, illustrating radiation attenuation as a function of shield thickness.

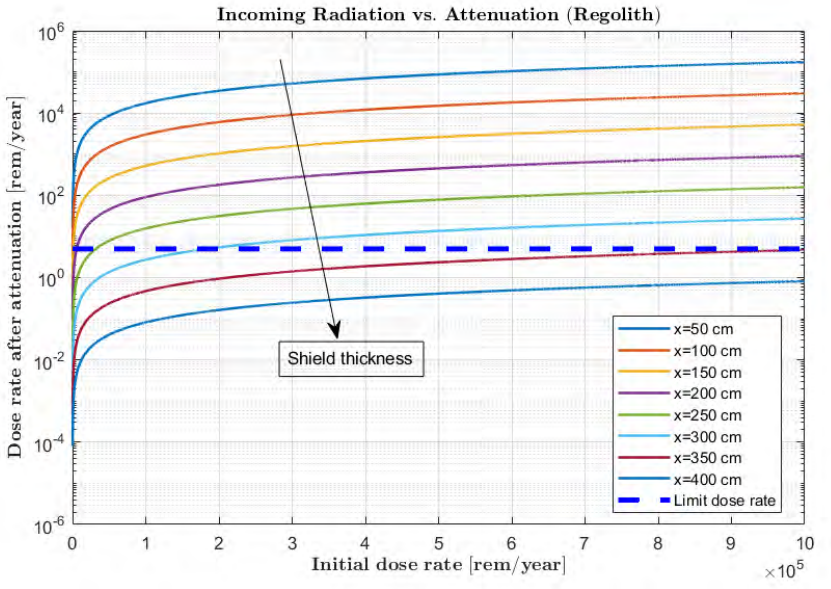

Figure 13. Dose rate after attenuation by regolith as a function of dose rate before attenuation, with different values of shield thickness. The higher the thickness, the higher the attenuation is at a fixed incoming dose rate.

S_3: Quadratic law in vacuum

The computation of D_{3n} is quite immediate, since all the other quantities appearing into the quadratic decay law for vacuum are known:

$$D_{3n} = D_{2n} \cdot \left(\frac{l_n}{l_n + r_{ext_n}} \right)^2.$$

3.5. Effects of the Cosmic Radiation

Once the radiation dose $D(x, y, z)$ from the nuclear reactors is known, it is essential to also consider cosmic radiation, given the Moon's nearly absent atmosphere. Therefore, using a safety threshold based solely on $D = 5$ rem/year, which accounts only for reactor radiation, would be an overly optimistic estimation. Instead, the following inequality should be used to identify the safe region, where D_{cr} and D_{Nr} represent the dose rates from cosmic radiation and nuclear reactors, respectively:

$$D_{cr}(x, y, z) + D_{Nr}(x, y, z) < 5 \text{ rem/y}. \tag{33}$$

According to [39], 60 µSiever per hour target the astronauts on the Moon. With this information, the following calculation can be made (remember that 1 rem = 0.01 Sievert):

$$\phi \left[\frac{\text{hours}}{\text{day}} \right] \cdot d \left[\frac{\text{days}}{\text{y}} \right] \cdot 60 \left[\frac{\mu\text{Sv}}{\text{hour}} \right] + D_{Nr} \left[\frac{\mu\text{Sv}}{\text{y}} \right] < 50,000 \left[\frac{\mu\text{Sv}}{\text{y}} \right]. \tag{34}$$

where ϕ and d, two additional degrees of freedom of the model, represent the number of cosmic radiation exposure hours per day and the number of exposure days per year. Since the aim is to guarantee a permanent stay on the Moon, d is taken as a fixed parameter, equal to 365 days. With this approach, the choice of ϕ affects the nuclear reactors' tolerated dose rate and consequently, the safety distance, as shown hereafter:

$$\begin{aligned} &\phi \cdot 365 \cdot 60 + D_{Nr} < 50{,}000 \\ &0 < D_{Nr} < 50{,}000 - 21{,}900 \cdot \phi. \end{aligned} \tag{35}$$

This leads to an important conclusion: on average, the theoretical maximum number of hours per day an astronaut can spend outside the habitat (which is assumed to be perfectly isolated) is given by $\phi = 2.28$, which is about 2 h and 17 min. If the average ϕ were higher, it would lead to a negative nuclear reactor dose of radiation, which is physically impossible. On the other hand, a decrease in ϕ causes the tolerated D_{Nr} to increase and the safety distance to get smaller.

4. Results from the Implementation of the Model

The illustrated model, including the shielding effect provided by regolith, is used to generate relevant results. As a matter of fact, some parametric studies were carried out, and their outcome is reported through this section.

First study: safety distance r_s vs. offset off (cosmic radiation included or not).

This first study is conducted with the aim of determining the effect of offset off on the minimum safety distance r_s required from the habitat. The fixed quantities of the model are as follows:

1. $N_r = 5$.
2. $P_{el} = P_{tot}/5 = 13$ kWe.
3. $\gamma = 5$ m.
4. $B = 3$ m.

5. $h = z - off = 10$ m (it means that r_s is computed by considering a minimum safety height of 10 m, that is over 10 m the radiation is not acceptable since it is greater than the limit).
6. $\phi = 1.5$ (it means a daily average exposure of 1 h 30 min per astronaut is considered, in order to have a margin with respect to the limit of 2 h 17 min).

The situation is analyzed under two different scenarios: one that includes the effect of cosmic radiation in the computation of safety distance and one that does not. As illustrated in Figure 14, when the additional requirement for cosmic radiation is considered and combined with the radiation dose from the reactors, the tolerated dose rate from the reactors must be lower, leading to a higher r_s. It is evident that in both scenarios, the relative gain decreases as the offset increases. In particular, as illustrated in Figure 15, it seems convenient to increase the offset from ground level within a range of (40–60) cm: beyond this interval, the gain in r_s is almost negligible, and the amount of regolith to be dug becomes too elevated with a consequent increase in power consumption. In fact, 2.26 m/cm and 1.10 m/cm are, respectively, the r_s gains for each cm dug for $off = 40$ cm and $off = 60$ cm.

A good trade-off could be an offset equal to 50 cm, corresponding to $r_s = 92$ m in case cosmic radiation is considered and $r_s = 85$ min case it is not. If these values are compared with the ones presented in Figure 6, for $N_r = 5$, the advantage of a shield is immediately clear: 2572 m are required without shields, against 92 m with a $\Delta r_s = 92 - 2572 = -2480$ m. The final safety distances will be refined with further studies, where the fixed degrees of freedom will play a role. From now on, however, the offset is assumed equal to 50 cm.

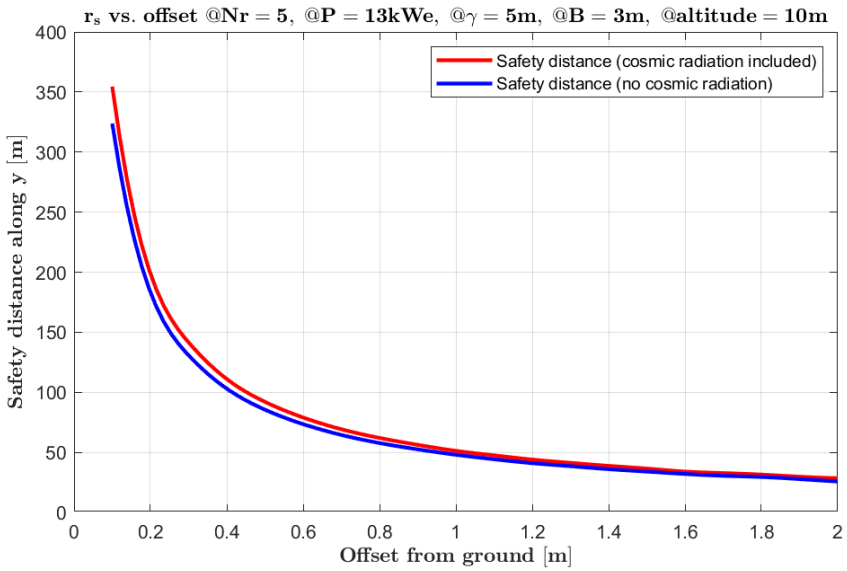

Figure 14. Safety distance as a function of offset (cosmic radiation yes and no).

Second study: effect of N_r at fixed total P_{el} on safety distance r_s (cosmic radiation included).

Since cosmic radiation is present on the Moon in every situation, this second study, and all the successive ones as well, assume its contribution in the calculation. The value of ϕ is set equal to 1.5 also here.

In this case the analysis aims at evaluating the effect of an increase in the number of reactors by keeping the total power generation constant and therefore scaling appropriately each reactor's supply on the safety distance. Here, the fixed quantities are as follows:

1. $off = 0.5$ m;
2. $B = 3$ m;
3. $\gamma = 5$ m;

4. Total power $P_{el} = 65$ kWe.

The safety threshold along z, as assumed in the first study, is set equal to $h = (z - off) = 10$ m. As shown in Figure 16, the effect is minimal. In fact, the value of r_s ranges from 90.7 m to 93.2 m for, respectively, $N_r = 8$ and $N_r = 2$. For practical reasons—such as increased reliability and lighter chambers—the analysis excludes plants with fewer than four reactors (where $N_r = 4$ corresponds to $r_s = 92.0$ m). Thus, the effect of varying N_r on r_s is not significant; increasing the number of reactors from four to eight only reduces the safety distance by $92.0 - 90.7 = 1.3$ m. While the number of reactors does not significantly impact safety requirements, the final configuration will be determined by additional factors such as system redundancy and maintenance accessibility.

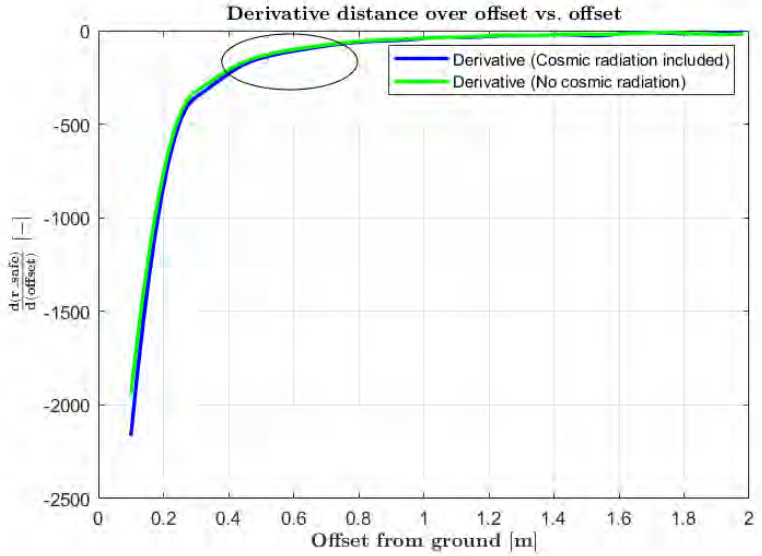

Figure 15. Derivative $\frac{d}{d(off)} r_s$. It gets negligible after $off = 0.6$ m.

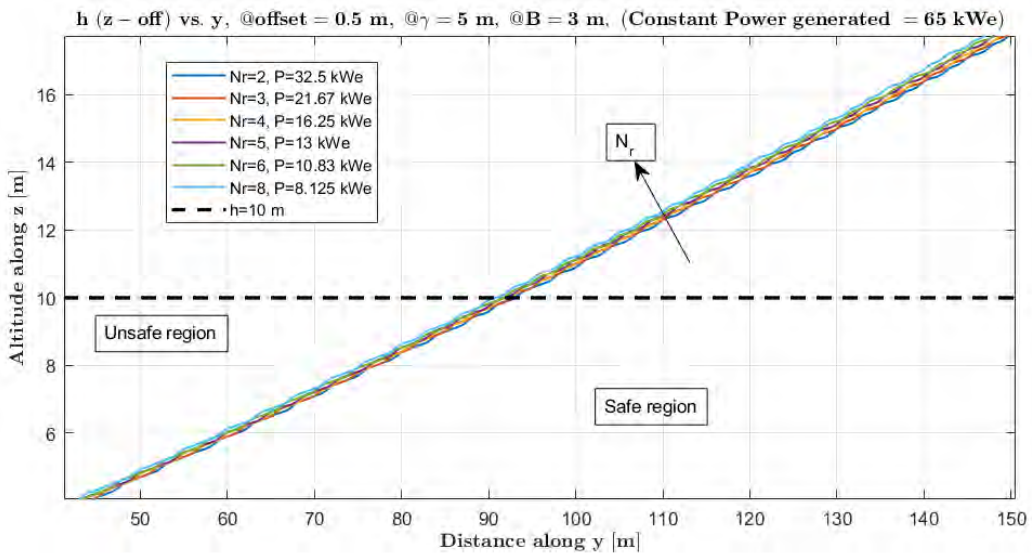

Figure 16. Effect of N_r on safety distance.

Third study: Effect of reactor inter-distance γ on r_s for different values of N_r.

It seems relevant to investigate the effect given by the spacing γ on the value of safety distance. Here, the fixed variables are as follows:

1. $off = 0.5$ m;

2. $B = 3$ m;
3. Total power $P_{el} = 65$ kWe.

It is evident that cosmic radiation is accounted for, with the safety distance r_s calculated based on a height of 10 m above ground level. On the basis of these assumptions, Figure 17 reveals two key findings:

1. For a fixed inter-reactor spacing γ, multiple smaller reactors provide better performance than fewer larger ones, confirming the results of the second study.
2. Increasing γ from 3 m to 20 m reduces r_s by only 6 m, indicating that reactor spacing has minimal impact on safety requirements.

Based on these results, the optimal configuration appears to be an 8-reactor plant with a 0.5 m offset and 20 m inter-reactor spacing, yielding a safety distance of $r_s = 86$ m. However, this configuration must be further evaluated against the energy costs associated with excavation for reactor placement.

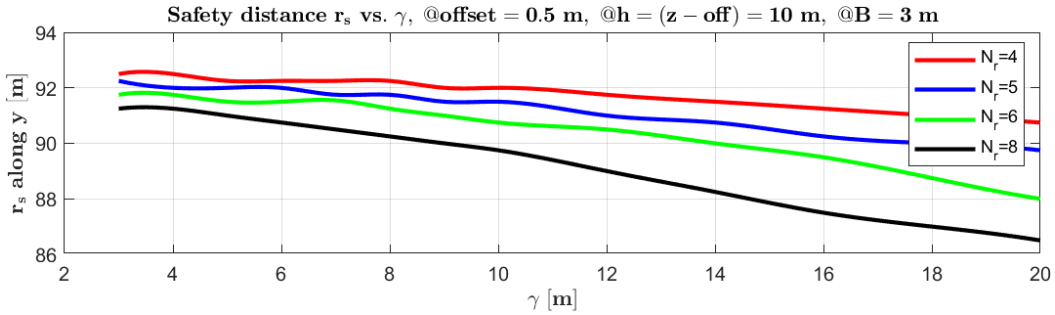

Figure 17. Effect of γ on safety distance for different N_r values.

Fourth study: Energy required to dig the hole.

A detailed and refined analysis involving the use of cost functions to find an optimum point for the size of the dip is beyond the aim of this paper. In spite of that, a preliminary study, involving the effect of γ on the energy required to dig, is carried out. Initially, it can be assumed that the total amount of energy needed (E_{req}) is proportional to the volume of regolith extracted (V_{reg}). In other words,

$$E_{req} \propto V_{reg}. \tag{36}$$

This can be justified by stating that the total energy may be written as the product of three terms: the number of excavator actions, the volume extracted for each action, and the energy per unit volume. The higher the overall volume is, the higher the number of actions (n_{acts}) (if the capacity of the hypothetical excavator is assumed as fixed). In the formula,

$$E_{req} = n_{acts} \cdot \frac{V}{act} \cdot \frac{E}{V} \implies E_{req} \propto V_{req}. \tag{37}$$

As regards the whole volume, the following formula can be derived (under the assumptions of a parallelepiped-shaped hole and a further spacing of $\gamma/2$ per each of the two external reactors along the line):

$$V_{reg} = (off + h_r) \cdot B \cdot \gamma N_r. \tag{38}$$

where h_r is the height of a reactor, from its base to its top. If all the reactors are equally sized and B is fixed to 3 m, it is finally obtained:

$$\frac{E_{req}}{E_{min}} = \frac{\gamma N_r}{\gamma_{min} N_{r,min}} = \frac{\gamma N_r}{3 \cdot 4} = \frac{\gamma N_r}{12}. \tag{39}$$

The minimum values for γ and N_r are chosen according to a physical intuition: $N_{r,min} = 4$ for what is stated in the second study, while $\gamma_{min} = 3$ m for practical reasons due to the reactor bulk extension. The ratio is plotted for different γ and N_r values in Figure 18. Here, it is obvious that an increase in γ and N_r causes the energy required for digging to increase as well.

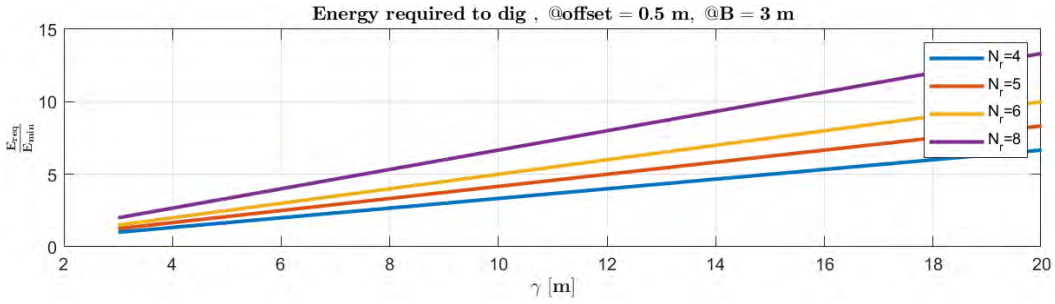

Figure 18. Ratio $\frac{E_{req}}{E_{min}}$ versus γ for different N_r values.

5. Results and Discussion

The sizing analysis yields several key insights:

1. Safety requirements and energy efficiency present competing objectives: reducing N_r and γ improves the energy consumption ratio $\frac{E_{req}}{E_{min}}$ but increases the safety distance r_s.
2. The minimal impact of γ and N_r on r_s suggests these parameters should be minimized while maintaining the following:
   (a) Physical space requirements for reactor installation;
   (b) Sufficient modularity for emergency management.
   (c) Feasible transportation logistics.
3. The dip width B should be minimized to reduce excavation volume and energy requirements ($V_{reg} \propto B$), while accommodating reactor dimensions.
4. Based on technical and standardization constraints, the recommended configuration is as follows:
   (a) Five to six reactors.
   (b) Inter-reactor spacing (measured along the x-axis): 3–5 m.
   (c) Dip width: 3 m (accommodating reactors up to 1.5 m radius).
   (d) Safety distance (measured along the y-axis): 90 m.

   While safety factors should be applied to account for model simplifications, the shielded configuration significantly reduces cable length and energy losses compared with unshielded alternatives while maintaining compliance with safety requirements. The depth of the hole, equal to $off + h_r$, is not provided since the only relevant contribution involved in the r_s assessment is given by off. The height of the reactor affects only the energy required to dig, among the variables considered in this study, which is certainly expected to depend on technology maturity and extraction capability constraints. However, the discussion concerning both excavation issues and associated costs is outside the aim of this work.

5. The general graphical outcome of the plant modeling in MATLAB R2024a is shown in Figure 19. For clarity, this figure does not depict the final configuration but rather illustrates the results from a random set of inputs. Displaying the actual final configuration would compress the curves too much, making the results less comprehensible. The figure includes the reactor positions and the iso-dose radiation surfaces, with the most tilted curve representing the most conservative approach, which accounts for cosmic radiation. This visualization helps to distinguish between safe and unsafe regions.
6. It is paramount to specify that the illustrated model is not validated through tests or experimental data. Its aim is to provide a theoretical proof of regolith shielding capabilities in the framework of protection against nuclear radiation and its implication on the design of a human settlement. Additional tests are required to ensure to what extent the results really adhere to reality.

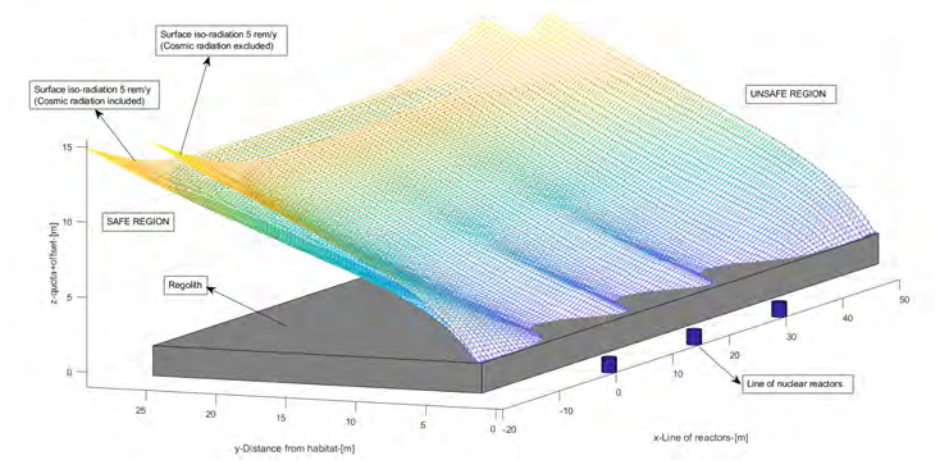

Figure 19. Surfaces iso-radiation resulting from the model.

5.1. Comparison Between Discussion Results and Existing Technologies

At the conclusion of this analysis, the literature data will be used to identify the reactor concept that best aligns with the results from the previous section. To aid in decision-making, Table 5 highlights the key elements that summarize the technical solutions implemented in the reactors previously reviewed. Based on these characteristics and the design developed in previous sections, the ideal reactor will be chosen, considering the features of the various reactors. This analysis will focus only on some factors, as this work aims to offer a solution from the perspective of an organic outpost design. Therefore, while technical details regarding core design, coolant, and fuel are provided, the emphasis will be on aspects most relevant to the outpost's design.

The evaluation criteria for the comparison include mass, power output, dimensions, modularity, and ISRU compatibility. Each reactor design presents distinct characteristics that warrant careful consideration.

The SC-SCORE reactor demonstrates exceptional performance in terms of specific mass ratio and offers an efficient integration with lunar regolith shielding. Its compact height minimizes excavation requirements, and the design incorporates robust passive safety features. However, its power output and limited modularity fall short of MOSS project requirements. The reactor's compact design architecture offers significant advantages in implementation efficiency, as its reduced height (h_r) minimizes the required excavation depth ($h_r + off$), directly optimizing volumetric energy requirements for site preparation.

Table 5. Key aspects of the presented reactors.

Characteristic	**LEGO [30]**	**FSP [32]**	**SC-SCORE [31]**
Power Output (kWe)	5	40	∼450
Mass (kg)	448 (unshielded)	7334	∼480
Specific Mass (kg/kWe)	89.6	183.5	∼1.1
Fuel	93% enriched UO_2	HALEU	92.7% enriched U_{235}
Coolant	Liquid Na	Liquid Na/NaK	Liquid NaK-56
Power Conversion	Stirling cycle	Stirling cycle	SiGe thermoelectric
Heat Rejection	Carbon–carbon composite heat pipe radiators	ISS-inspired	Rubidium heat pipe radiators
Core Design	Hexagonal, 84 fuel rods, 43 heat pipes	-	Monolithic solid core, six sectors, cylindrical axial cavities
Moderator	-	Yttrium hydride (YH)	-
Reflector	Lunar Regolith	-	Berillium Oxide (BeO)
Height (m)	8.77	17.6	3.5 (no radiators)
Diameter (m)	0.50 (with radiators)	3.2	-
Modularity	Subcritical subunits, clustered for criticality	Three separate deployable elements	Six hydraulically independent sectors
Shielding	Lunar regolith	Distance from outpost	Lunar regolith
Estimated Lifetime (yr)	>5	10	21
Key Advantages	Inherently sub-critical design, scalable, uses proven materials, efficient heat management, utilizes lunar regolith for shielding	Deployable design, uses HALEU fuel, based on flight-qualified components, efficient heat rejection system	Highly reliable, passive safety features, negative temperature reactivity feedback, avoids single point failures

The LEGO reactor excels through its modular design approach and innovative use of lunar regolith for both shielding and neutron reflection. This dual utilization of local resources could significantly reduce Earth-launched mass, potentially offsetting its higher specific mass compared with SC-SCORE. However, the greater excavation depth requirements present a notable challenge for implementation. The design's emphasis on modularity and efficient use of in situ resources represents a significant advancement in lunar reactor technology, particularly in its approach to radiation shielding and neutron reflection.

The FSP reactor, being the most recent design, introduces several modern innovations, including an integrated mobility platform and a modular three-platform configuration. Its power output and configuration (6 reactors, 40 kWe) align closely with MOSS requirements, and it benefits from component validation through the 2018 KRUSTY test. The design demonstrates superior alignment with the project's core requirements, particularly in terms of operational parameters and power specifications. However, its larger dimensional footprint and higher launch mass present logistical challenges. Most critically, its surface installation design conflicts with established safety requirements, necessitating excessive distance from the habitat.

A comprehensive analysis of these alternatives reveals distinct trade-offs. While FSP provides the closest match to our power and operational requirements, its surface-based installation protocol presents fundamental safety limitations. SC-SCORE's compact

design offers crucial advantages in implementation and energy efficiency, though it lacks the necessary power output. LEGO's innovative approach to modularity and resource utilization represents important principles for future design considerations.

The optimal solution for the MOSS project would therefore integrate three key design elements: FSP's power output specifications and reactor configuration, which perfectly match our operational requirements; SC-SCORE's compact dimensional profile, which minimizes installation energy requirements and optimizes safety through burial; and LEGO's modular architecture and regolith utilization strategy, which enhances operational flexibility and resource efficiency. This synthesis of design elements would create a reactor system that optimally balances power generation, installation efficiency, and operational flexibility while maintaining compliance with all safety requirements.

5.2. Final Remarks and Future Developments

Future work should refine parametric studies to explore alternative reactor configurations, which could bring reactors closer to the outpost, reduce wiring needs, and facilitate supply logistics while preserving base safety. Additionally, while not considered here, fission reactors designed for terrestrial applications could be studied for potential adaptation to the lunar surface.

6. Conclusions

This study has provided a detailed analysis of reactor configurations for the MOSS project, with a focus on optimizing the balance between safety, energy efficiency, and operational feasibility. The results suggest that the most effective configuration involves five to six reactors with a three-meter dip width and a safety distance of 90 m. This design minimizes energy losses while maintaining the necessary safety margins.

When comparing existing reactor concepts—SC-SCORE, LEGO, and FSP—distinct trade-offs emerge. SC-SCORE's compact design and passive safety features offer significant advantages in energy efficiency and safety, though it falls short in power output. LEGO's modular approach and innovative use of lunar regolith for shielding present a promising solution for resource utilization but require deeper excavation. FSP, while aligning with the power output needs and operational requirements of MOSS, introduces challenges related to safety due to its surface installation design.

The most effective reactor solution for the MOSS project would combine the strengths of these three concepts: FSP's power output and reactor configuration, SC-SCORE's compactness to reduce excavation needs and optimize safety, and LEGO's modularity and utilization of lunar regolith. This integrated approach would offer a balance of power generation, installation efficiency, and operational flexibility, ensuring that the MOSS project meets its energy requirements while adhering to safety and logistical constraints.

Further experimental validation and testing are necessary to ensure that these proposed configurations will perform as expected in real-world conditions. In particular, additional attention must be paid to excavation techniques, long-term operational reliability, and safety margins. Ultimately, the findings from this study contribute to advancing the development of an efficient, scalable, and safe energy solution for lunar settlements, supporting the broader goals of the MOSS project.

Author Contributions: Conceptualization, M.M. and L.P.; methodology, M.M., C.G.F., and L.P.; software, M.M. and L.P.; validation, M.M.; formal analysis, M.M. and L.P.; investigation, M.M., C.G.F., and L.P.; resources, C.G.F.; data curation, M.M. and L.P.; writing—original draft preparation, M.M. and L.P.; writing—review and editing, M.M., C.G.F., and L.P.; visualization, M.M.; supervision, C.G.F.; project administration, C.G.F.; funding acquisition, C.G.F. All authors have read and agreed to the published version of the manuscript.

Funding: This research received no external funding.

Institutional Review Board Statement: Not applicable.

Data Availability Statement: The original contributions presented in this study are included in the article. Further inquiries can be directed to the corresponding author.

Acknowledgments: The authors would like to extend their sincere gratitude to the entire MOSS team for their invaluable contributions, dedication, and collaborative spirit throughout this project. Your expertise and commitment have been instrumental in driving the research forward and ensuring its success. This work stands as a testament to the power of teamwork and interdisciplinary cooperation.

Conflicts of Interest: The authors declare no conflicts of interest.

References

1. Smith, M.; Craig, D.; Herrmann, N.; Mahoney, E.; Krezel, J.; McIntyre, N.; Goodliff, K. The Artemis Program: An Overview of NASA's Activities to Return Humans to the Moon. In Proceedings of the 2020 IEEE Aerospace Conference, Big Sky, MT, USA, 7–14 March 2020; pp. 1–10. [CrossRef]
2. NASA. FAQ: NASA's Artemis Campaign and Recent Updates. 2024. Available online: https://www.nasa.gov/general/faq-nasas-artemis-campaign-and-recent-updates/ (accessed on 4 January 2025).
3. SpaceNews. China on Track for Crewed Moon Landing by 2030, Space Official Says. *SpaceNews*, 4 January 2024. Available online: https://spacenews.com/china-on-track-for-crewed-moon-landing-by-2030-space-official-says/ (accessed on 4 January 2025).
4. European Space Agency. Argonaut Lunar Lander. 2023. Available online: https://www.esa.int/Science_Exploration/Human_and_Robotic_Exploration/Exploration/Argonaut (accessed on 4 January 2025).
5. Kuthunur, S. ESA Targets 2031 for 1st Argonaut Moon Lander Mission. 2024. Available online: https://www.space.com (accessed on 4 January 2025).
6. Japan Aerospace Exploration Agency. The Future of Human Space Exploration—To the Moon, Mars, and Beyond. 2023. Available online: https://humans-in-space.jaxa.jp/en/future/ (accessed on 4 January 2025).
7. Press Information Bureau. Prime Minister Reviews Readiness of Gaganyaan Mission. 2025. Available online: https://pib.gov.in/PressReleseDetailm.aspx?PRID=1968368&reg=3&lang=1 (accessed on 4 January 2025).
8. Ross, A.K.; Ruppert, S.; Gläser, P.; Elvis, M. Preliminary quantification of the available solar power near the lunar South Pole. *Acta Astronaut.* **2023**, *211*, 616–630. [CrossRef]
9. Colozza, A.J. *Small Lunar Base Camp and In Situ Resource Utilization Oxygen Production Facility Power System Comparison*; Technical Report NASA/TM-2020-220567; NASA Glenn Research Center: Cleveland, OH, USA, 2020.
10. Mihailescu, E. *Transformers for Extreme Environments*; Technical Report; NASA: Washington, DC, USA, 2016.
11. Gibson, M.; Oleson, S.; Poston, D.; McClure, P. NASA's Kilopower reactor development and the path to higher power missions. In Proceedings of the 2017 IEEE Aerospace Conference, Big Sky, MT, USA, 4–11 March 2017; pp. 1–14. [CrossRef]
12. OHB Czechspace RocketRoll: Preliminary European Reckon on Nuclear Electric Propulsion for Space Applications. Project Overview. 2023. Available online: https://www.ohb-czech.cz/our-projects/nep-rocketroll (accessed on 4 January 2024).
13. Larson, W.J.; Pranke, L.K. *Human Spaceflight: Mission Analysis and Design*; McGraw-Hill College: New York, NY, USA, 1999.
14. Jones, H. *Power Management for Space Advanced Life Support Systems*; SAE Technical Paper 2002-01-2397; SAE: Warrendale, PA, USA, 2002. [CrossRef]
15. Haridas, A.; Rao, R.; Farrar, C. Structural Health Monitoring (SHM) in Space Applications: A Review. *J. Aerosp. Eng.* **2021**, *34*. [CrossRef]
16. Molteni, C. Preliminary Architecture of Nuclear Space Reactor for a Lunar Base. Master's Thesis, Politecnico di Milano, Milano, Italy, 2022.
17. Kaczmarzyk, M.; Musiał, M. Parametric Study of a Lunar Base Power Systems. *Energies* **2021**, *14*, 1141. [CrossRef]
18. Nomenclature for Planetary System, International Astronomical Union Working Group for Nomenclature for Planetary System. Shackleton. Planetary Names: Gazetteer of Planetary Nomenclature. 2024. Available online: https://planetarynames.wr.usgs.gov/Feature/5450 (accessed on 4 January 2025).
19. Wilson, R.; Smith, J. Fundamentals of Reactor Thermal Power Generation. *Nucl. Eng. Int.* **2024**, *66*, 28–34.
20. Bubelis, E. *Conceptual Designs of PHTS, ESS and PCS for DEMO BoP with Helium Cooled BB Concept*; Technical Report EFDA_D_2M9JM7; EUROfusion: Garching, Germany, 2018.
21. Demuth, S.F. SP100 space reactor design. *Prog. Nucl. Energy* **2003**, *42*, 323–359. [CrossRef]
22. Poston, D.I. The Heatpipe-Operated Mars Exploration Reactor (HOMER). In Proceedings of the Space Technology and Applications International Forum—2001, Albuquerque, NM, USA, 11–14 February 2001; American Institute of Physics Conference Series; El-Genk, M.S., Ed.; AIP: Melville, NY, USA, 2001; Volume 552, pp. 797–804. [CrossRef]

23. Poston, D.I. *Nuclear Design of the SAFE-400a Space Fission Reactor*; Technical Report LA-UR-02-1974; Los Alamos National Laboratory: Los Alamos NM, USA, 2002.
24. Black, D.; Mowery, A., Space Power Annular Reactor System. In Proceedings of the 39th AIAA/ASME/SAE/ASEE Joint Propulsion Conference and Exhibit, Huntsville, AL, USA, 20–23 July 2003; ARC: Reston, VA, USA, 2012; Chapter 1, p. 11, [CrossRef]
25. Bushman, A.; Carpenter, D.; Ellis, T.; Gallagher, S.; Hershcovitch, M.; Hine, M.; Johnson, E.; Kane, S.; Presley, M.; Roach, A.; et al. *The Martian Surface Reactor: An Advanced Nuclear Power Station for Manned Extraterrestrial Exploration*; Technical Report; MIT: Cambridge, MA, USA, 2011.
26. El-Genk, M.S.; Tournier, J.M.P. SAIRS—Scalable Amtec Integrated Reactor space power System. *Prog. Nucl. Energy* **2004**, *45*, 25–69. [CrossRef]
27. Tournier, J.M.P.; El-Genk, M.S. Reactor Lithium Heat Pipes for HP-STMCs Space Reactor Power System. *AIP Conf. Proc.* **2004**, *699*, 781–792. [CrossRef]
28. King, J.C.; El-Genk, M.S. Solid-Core, Gas-Cooled Reactor for Space and Surface Power. *AIP Conf. Proc.* **2006**, *813*, 298–307. [CrossRef]
29. Powell, J.; Maise, G.; Paniagua, J. SUSEE—Ultra light nuclear space power using the steam cycle. In Proceedings of the 2003 IEEE Aerospace Conference Proceedings (Cat. No.03TH8652), Big Sky, MT, USA, 8–15 March 2003; Volume 1, pp. 1–507. [CrossRef]
30. Bess, J. A Basic LEGO Reactor Design for the Provision of Lunar Surface Power. In Proceedings of the International Conference on Advances in Nuclear Power Plants, ICAPP 2008, Anaheim, CA, USA, 8–12 June 2008.
31. Schriener, T.; El-Genk, M. Safety analysis of Solid Core-Sectored Compact Reactor (SC-SCoRe). In Proceedings of the International Congress on Advances in Nuclear Power Plants, ICAPP 2014, Charlotte, NC, USA, 6–9 April 2014; Volume 3, pp. 1714–1724.
32. Oleson, S.; Packard, T.; Turnbull, E.; Gibson, M.; Rao, D.; Barth, C.; Wilson, S.; Schmitz, P.; Colozza, A.; Klefman, B.; et al. A Deployable 40 kWe Lunar Fission Surface Power Concept. In Proceedings of the NASA Technical Reports Server (NTRS), Cleveland, OH, USA, 8–12 May 2022; pp. 519–527. [CrossRef]
33. Mazzoldi, P. *Fisica: Elettromagnetismo e onde*; EdiSES: Naples, Italy, 2021.
34. *Standards for Protection Against Radiation*; Code of Federal Regulations, 10 CFR Part 20; U.S. Nuclear Regulatory Commission: Washington, DC, USA, 1991. Available online: https://www.nrc.gov/reading-rm/doc-collections/cfr/part020/full-text.html (accessed on 4 January 2024).
35. Miller, J. Radiation shielding properties of lunar regolith and regolith simulant. Technical report. In Proceedings of the NLSI Lunar Science Conference, Moffett Field, CA, USA, 20–23 July 2008.
36. Iborra, A. *Spacecraft Thermal Loads*; Technical Report; European Space Agency: Paris, France, 2023.
37. National Institute of Standards and Technology. X-Ray Mass Attenuation Coefficients. 2004. Available online: https://www.nist.gov/pml/x-ray-mass-attenuation-coefficients (accessed on 4 January 2025).
38. Heiken, G.H.; Vaniman, D.T.; French, B.M. *Lunar Sourcebook*; Cambridge University Press: Cambridge, UK, 1991.
39. Wall, M. We Now Know Exactly How Much Radiation Astronauts Will Face on the Moon. 2020. Available online: https://www.space.com/ (accessed on 4 January 2025).